Preprint typeset using LaTeX style emulateapj v. 5/2/11

arXiv:1702.01382v1 [astro-ph.HE] 5 Feb 2017

EXTREMELY BRIGHT GRB 160625B WITH MULTI-EPISODES EMISSION: EVIDENCES FOR LONG-TERM EJECTA EVOLUTION

Hou-Jun Lü[1], Jing Lü [1], Shu-Qing Zhong[1], Xiao-Li Huang[1], Hai-Ming Zhang[1], Wei Xie[2], Rui-Jing Lu[1], and En-Wei Liang[1]

ABSTRACT

GRB 160625B is an extremely bright GRB with three distinct emission episodes. By analyzing its data observed with the GBM and LAT on board the *Fermi* mission, we show that the spectrum of its initial short episode (Episode I) can be fitted with a multi-color black body (mBB) model, and the derived maximum temperature ($T_{\rm max}$) is ~ 25 keV. The time-resolved spectra of its main episode (Episode II), which was detected with both GBM and LAT after a long quiet stage (~ 180 seconds) after the initial episode, can be fitted with a model composing of an mBB component plus a cutoff power-law (CPL) component. The derived $T_{\rm max}$ initially increases up to ~ 1100 keV, then decays down to ~ 300 keV. The photon index and the cutoff energy of the CPL component do not show clear evolution trend. This GRB was detected again in the GBM and LAT bands with a long extended emission (Episode III) after a quiet period of ~ 300 seconds. The spectrum of Episode III is adequately fitted with a CPL plus a single power-law models, and no mBB component is required. These features may imply that the emission of three episodes are dominated by distinct physics process, i.e., Episode I is possible from cocoon emission surrounding the relativistic jet, Episode II is from photosphere emission and internal shock of relativistic jet, and Episode III is contributed by internal and external shocks of relativistic jet. On the other hand, both X-ray and optical afterglows are consistent with standard external shocks model.

Subject headings: gamma rays burst: individual (160625B)

1. INTRODUCTION

Long duration gamma-ray bursts (GRBs) are thought to be caused by a core-collapse of massive star (Woosley 1993; Paczyński 1998), which is also supported by several lines of observational evidence. (1) A handful of long GRBs are associated with Type Ic supernovae (Galama et al. 1998; Stanek et al. 2003; Woosley & Bloom 2006). (2) The host galaxies of long GRBs are in intense star formation galaxies (Fruchter et al. 2006). Following the collapse, a black hole or magnetar central engine is formed and it powers a ultra-relativistic jet (Usov 1992; Thompson 1994; Dai & Lu 1998; Popham et al. 1999; Narayan et al. 2001; Lei et al. 2013; Lü & Zhang 2014).

Numerical simulations show that a relativistic jet can be launched successfully, and it breaks out the stellar envelope of the progenitor star (MacFadyen & Woosley 1999; Zhang et al. 2003; Morsony et al. 2007; Mizuta & Ioka 2013; Geng et al. 2016). On the other hand, if the mass density of collimated outflow is less than that of the stellar envelope. A "cocoon" component is an inevitable product when the jet propagate within the stellar envelope (Ramirez-Ruiz et al. 2002; Lazzati & Begelman 2010; Nakar & Piran 2017). The wasted energy of jet is recycled into a high pressure cocoon surrounding the relativistic jet (Ramirez-Ruiz et al. 2002; Lazzati & Begelman 2005). The gained energy of cocoon is comparable with that released energy of observed GRB. So that, the emission from the cocoon has been invoked to be as explanation of the thermal emission of GRBs (Fan et al. 2006; Ghisellini et al. 2007; Piro et al. 2014), or the precursors emission and the steep decay in the early X-ray afterglow of GRBs (Ramirez-Ruiz et al. 2002; Pe'er et al. 2006; Lazzati et al. 2010). Theoretically, Ramirez-Ruiz et al. (2002) proposed that a γ-ray and X-ray transients with a short duration may be produced from the cocoon emission. Lazzati et al.(2010) suggested that the transients may be seen similar to a short GRB by an observer at wide angles. Nakar & Piran (2017) proposed that a possible signatures (γ-ray, X-ray and optical) of the cocoon emission may be detected, but it is strongly dependence on the level of mixing between shocked jet cocoon and shocked stellar cocoon. In any case, the cocoon emission was also expected that it has a thermal component of observed spectrum in above models (Ramirez-Ruiz et al. 2002; Lazzati & Begelman 2005).

After the jet breaks out the star envelope, the outflow of relativistic jet produces the prompt γ-ray emission getting through the internal shocks or magnetic dissipation when it become optically thin (Mészáros & Rees 1993; Piran et al. 1993; Rees & Mészáros 1994; Zhang & Yan 2011). Within the matter-dominated fireball scenario, it was expected that an observed GRB spectrum should be composed of a thermal component from the photosphere emission and a non-thermal component from the synchrotron radiations of relativistic electrons in the internal shock regions (Mészáros & Rees 2000; Rees & Mészáros 2005; Pe'er et al. 2006; Giannios 2008; Beloborodov 2010; Lazzati & Begelman 2010). Therefore, a bright black body component should be detectable. After that, a multi-wavelength afterglow emission is produced when the fireball (outflow) propagates into the circum medium (Mészáros & Rees 1997; Sari et al. 1998; Zhang & Kobayashi 2005; Fan & Piran 2006; Gao et al. 2013).

From observational point of view, only 10% GRBs have

[1] Guangxi Key Laboratory for Relativistic Astrophysics, Department of Physics, Guangxi University, Nanning 530004, China; lhj@gxu.edu.edu; lew@gxu.edu.cn

[2] School of Physics, Huazhong University of Science and Technology, Wuhan 430074, China

a precursor emission component, and the spectra properties of precursors and main outbursts do not show any statistical difference (Troja et al. 2010; Hu et al. 2014). On the other hand, the GRBs with precursors are not substantial difference from the other GRBs without precursors (Troja et al. 2010; Hu et al. 2014). Those results suggested that the precursor would be the same emission component with the fireball.

Recently, an extremely bright GRB 160625B was detected by *Fermi* Gamma-Ray Burst Monitor (GBM) and Large Area Telescope (LAT), and measured redshift $z = 1.406$ (Xu et al. 2016). Its prompt γ-ray lightcurve is composed of three episodes: a short precursor, a very bright main emission episode, and a weak emission episode. The three episodes emission are separated by two long quiescent intervals (Zhang et al. 2016). Interestingly, Zhang et al. (2016) found that a pure thermal spectral component and non-thermal spectrum (known as Band function; Band et al. 1993) are existed in the precursor and main emission episodes, respectively. They suggested that the thermal component is from the photosphere emission of a fireball, and non-thermal component is from a Poynting-flux-dominated outflow. However, it is inconceivable that the transition from fireball to Poynting-flux-dominated jet lasts that long quiescent stage. In this paper, by reanalysing the multi-wavelength data of GRB 160625B, we propose that the precursor and main emission may be origin from different physics process, i.e., cocoon emission surrounding a jet and relativistic jet. Then, we also explore its long term evolution of ejecta.

This paper is organized as follows: the data reduction and data analysis are presented in §2 and §3. In §4, we derive The ejecta properties from the data. Conclusions and discussion are reported in §5 and §6. We adopt convention $F_\nu(t) \propto t^\alpha \nu^\beta$ through out the paper.

2. DATA REDUCTION

GRB 160625B triggered the *Fermi*/GBM at 22:40:16.28 UT on 25 June 2016 (T_0) for the first time (Burns 2016). This GRB was also detected by Konus-Wind (Svinkin et al. 2016). It is the brightest event observed by Konus-Wind for more than 21 years of its GRB observations (Svinkin et al. 2016). Interestingly, the *Fermi*/LAT was also triggered by this burst at $T_0 + 188.54$ seconds (Dirirsa et al. 2016), and more than 300 photons with energy above 100 MeV were detected. The highest photon energy is about 15 GeV (Dirirsa et al. 2016; Zhang et al. 2016). This GRB triggered GBM again at $T_0 + 660$ seconds.

We download the GBM and LAT data of GRB 160625B from the public science support center at the official *Fermi* Web site[3]. GBM has 12 sodium iodide (NaI) detectors covering an energy range from 8 keV to 1 MeV, and two bismuth germanate (BGO) scintillation detectors sensitive to higher energies between 200 keV and 40 MeV (Meegan et al. 2009). We select the brightest NaI and BGO detectors for the analyses. The spectra of this source are extracted from the TTE data and the background spectra of the GBM data are extracted from the CSPEC format data with user-defined intervals before and after the prompt emission phase. We reduce the LAT data using the LAT ScienceTools-v9r27p1 package and the P7TRANSIENT V6 response function (detailed information for the LAT GRB analysis are available in the NASA Fermi Web site). Two types of LAT data are available, i.e., the LAT Low Energy (LLE) data in the 100 MeV-100 GeV band and the high energy LAT data in the 0.02-300 GeV band. We extract the lightcurves and spectra of GRB 160625B from the GBM and LAT data.

Follow-up observation with the X-ray telescope (XRT) on board *Swift* was performed between $T_0 + 9.6$ ks and $T_0 + 10.0$ ks (Melandri et al. 2016). The *Swift*/XRT light curve and spectrum are extracted from the UK *Swift* Science Data Center at the University of Leicester[4]. A bright optical flare at the main prompt gamma-ray episode was detected with Mini-Mega TORTORA nine-channel wide-field monitoring system and other optical telescopes. We collect the optical data from Zhang et al. (2016).

3. DATA ANALYSIS

3.1. *Prompt Emission*

Figure 1 shows the lightcurves of the prompt and very early optical afterglow emission of GRB 160625B. The GBM-NaI lightcurve has three distinct episodes with 1 second time bin. The first episode lasts about one second (Episode I). The inset in the top panel of Figure 1 shows the lightcurve in 64 ms time-bin. One can find that it is a single pulse with rapidly rising and decaying. It was not detected with GBM-BGO and LAT. The source was in a quiescent stage with a duration of about 180 seconds without detection of any gamma-rays in the GBM and LAT bands. An extremely bright gamma-ray outburst with multiple peaks (Episode II) triggered Fermi-LAT and were also observed with GBM and even in the optical band since $T_0 + 187$ seconds. The source was in quiescent again and triggered GBM at $T_0 + 520$ seconds. The emission in this episode (Episode III) was detected with GBM-NaI detector and LAT. The lightcurve of this episode features as a long-lasting, low flux-level episode, similar to the extended emission (EE) component (e.g., Hu et al. 2014). Its duration is 372 seconds. Therefore, GRB 160625B experiences a short precursor, a main burst, and a long-lasting extended emission stages. The initial three data points of the V band lightcurve of the optical flare observed during the Episode II with the Mini-Mega TORTORA system is very spike. It rapidly increases to the peak brightness ($V = 8.04$ magnitude) at $T_0 + 200.3$ seconds with a slope of $\alpha_1 \sim 20$, then drops with a slope of $\alpha_2 \sim -15$ after the peak. The optical flux then transits to a decay phase with a slope of $\alpha_3 \sim -3.41$.

We jointly analyze the spectra observed with different detectors/telescopes for the three emission episodes of the prompt gamma-rays. We do not make the spectral fit with the empirical Band function (Band et al. 1993), but use an empirical model motivated by the standard fireball models. In general, a single black body is invoked to describe the photosphere emission (Rees & Mészáros 2005; Pe'er et al. 2006; Giannios 2008; Beloborodov 2010; Wang et al. 2016). In fact, it should be contributed by superposition of various black body radiation, namely, a multi-color black body (mBB) is more

[3] http://fermi.gsfc.nasa.gov/ssc/data/

[4] http://www.swift.ac.uk/results.shtml

convinced (e.g., Ryde et al. 2010; Lazzati & Begelman 2010; Pe'er & Ryde 2011; Lundman et al. 2013). In the framework of the fireball model, the observed spectrum of prompt gamma-rays should be composed of an mBB component from the photosphere emission and a non-thermal emission component from the optically thin internal shock region (e.g., Mészáros & Rees 2000). We adopt the mBB model as that used in Ryde et al. (2010), i.e.,

$$F_{\rm mBB}(E,T_{\rm max}) = \int_{T_{\rm min}}^{T_{\rm max}} \frac{dA(T)}{dT}\frac{E^3}{\exp[{\rm E/kT}]-1}, \quad (1)$$

where $T_{\rm max}$ and $T_{\rm mim}$ are free parameters, and $F(T) = \frac{\pi^4}{15}A(T)T^4$, $A(T)$ is the normalization. We assume that the flux of thermal component is power-law distribution with temperature, which read as

$$F(T) = F_{\rm max}(\frac{T}{T_{\rm max}})^q, \quad (2)$$

and q measures the power-law distribution of the temperature. We describe the non-thermal emission component with a CPL model, i.e., $F_{\rm nonth} = F_0 E^{-\Gamma_{\rm c}} e^{-E/E_{\rm c}}$.

We make spectral fit with the Xspec package and evaluate the goodness of our fits with the maximum likelihood-based statistics, so-called PGSTAT (Cash 1979). Figure 2 shows the observed νf_ν spectrum of Episode I in the GBM energy band. It was detected only by the NaI detector (see Figure 1). We find that the mBB model is adequate to fit the spectrum. One has $T_{\rm max} = 25.2 \pm 1.1$ keV, $T_{\rm min} = 3.45 \pm 1.26$ keV, and $q = 0.63 \pm 0.2$. The time-integrated spectrum of Episode II can not be fitted with the mBB plus CPL model. We extract its time-resolved spectra in 14 time-slices and find that they are well fitted with the mBB plus CPL model. Our results are reported in Table 1 and shown in Figure 6. It is observed that the mBB component is dominated the emission in the range of tens to hundreds of keVs, and both the emission in several keVs and MeVs are attributed to the CPL component. The $T_{\rm max}$ initially rapidly increases with time from 643 ± 67 keV to 1096^{+22}_{-23} keV, then gradually decays to $250 - 350$ keV. The power-law index q varies from 0.60 to 1.05. For the CPL component, we do not find any clear temporal evolution feature of $\Gamma_{\rm c}$, which are in the ranges of $\Gamma_c \in (1.27, 1.69)$. Figure 4 shows the temporal evolution of $T_{\rm max}$, $T_{\rm min}$, and $E_{\rm c}$.

Note that the bright optical flare was simultaneously detected in the Episode II. It peaks at $T_0+ \sim 200$ seconds with a exposure time of 10 seconds. We show the model curves derived from our fit for the spectrum observed in the time slice [195-205] seconds in comparison with the peak optical flux in Figure 5. Here, the optical data is corrected by the extinction of the Milk Way Galaxy ($A_V = 0.349$), but is not corrected for the extinction by the GRB host galaxy due to uncertainly extinction curves. It is found that the optical flux is higher than the model result with a factor of 3. Therefore, it may be contributed by both prompt optical emission and the reverse shocks, as we will discuss below.

Although the duration of Episode III is long, its flux is low. We do not make time-resolved analysis for this episode. We derive its time-integrated spectrum, which is shown in Figure 6. It is found that the emission in the LAT energy band is dominated by an extra power-law (PL) component. The spectrum cannot be fitted with the mBB+CPL model. Therefore, we use a CPL plus a single PL model to fit the data. One has $\Gamma_{\rm c} = 1.64 \pm 0.05$, $E_{\rm c} = 0.69 \pm 0.58$ GeV, and the index of the single PL component is 1.98 ± 0.5.

3.2. *Late Afterglows*

Both optical and X-ray afterglows were detected with XRT and UVOT onboard *Swift* and ground-based telescopes since $T_0 + 10^4$ seconds. Their lightcurves show similar features (Figure 7). The later optical afterglow light curve can be well fitted with a smooth broken power-law function, $F = F_0[(\frac{t}{t_b})^{\omega\alpha_1} + (\frac{t}{t_b})^{\omega\alpha_2}]^{1/\omega}$, and we fixed $\omega = 1/3$, which describes the sharpness of the break (Liang et al. 2007). Derived parameters are $\alpha_{\rm O,1} = -0.92 \pm 0.04$, $\alpha_{\rm O,2} = -2.30 \pm 0.51$, $t_{\rm O,b} = (2.33 \pm 0.40) \times 10^6$ seconds. The X-ray light curve also can be fitted with this function with parameters $\alpha_{\rm X,1} = -1.31 \pm 0.02$, $\alpha_{\rm X,2} = -2.38 \pm 0.75$, $t_{\rm X,b} = 2.33 \times 10^6$ seconds (fixed). The achromatic breaks should be due to the jet effect (Rhoads 1997).

We jointly fit the afterglow spectra in the optical-X-ray band in four selected time slices as marked in Figure 7. By correcting the extinction for the optical data and fixing the neutral hydrogen absorption for the soft X-rays of our Galaxy as $N_{\rm H} = 9.76 \times 10^{20}$ cm^{-2}, we find that a single power-law function is adequate to fit the spectra, yielding photon indices $\Gamma = -1.72 \pm 0.02$, -1.70 ± 0.02, -1.76 ± 0.04 and -1.85 ± 0.03 for the spectra derived from the four selected time slices. Extinction of the GRB host galaxy is negligible in our fits. Our results are shown in Figure 8. The observed flux slope and the photon index are roughly satisfied with the closure relation $\alpha \sim 3\beta/2$, where $\beta = \Gamma - 1$. This suggests that both the X-ray and optical afterglow should be in the spectral regime of $\nu_m < \nu < \nu_c$, where ν_m and ν_c are the characteristic frequencies of the synchrotron radiation of the relativistic electrons.

4. DERIVATION OF THE EJECTA PROPERTIES WITHIN THE FIREBALL MODELS

4.1. *Lorentz Factor and Radius of the GRB photosphere*

We estimate the $\Gamma_{\rm ph}$ values and radius of the GRB photosphere with the mBB component derived from our spectral fits in different emission episodes. We estimate the $\Gamma_{\rm ph}$ of photosphere emission with Pe'er et al. (2007),

$$\Gamma_{\rm ph} = [(0.16)(1+z)^2 D_{\rm L}\frac{Y\sigma_{\rm T}F^{\rm obs}}{2m_{\rm p}c^3\Re}]^{1/4}, \quad (3)$$

where $D_{\rm L}$ is the luminosity distance, $m_{\rm p}$ is the proton mass, $\sigma_{\rm T}$ is the Thomson scattering cross section, Y is the ratio between total fireball energy and energy radiated in the γ-ray band, which is fix at $Y = 1$ in our calculation, and $F^{\rm obs}$ is the total observed flux of both the thermal ($F^{\rm obs}_{\rm BB}$) and non-thermal ($F^{\rm obs}_{\rm non-BB}$) components. $\Re$ is defined as

$$\Re = (\frac{F^{\rm obs}_{\rm BB}}{\sigma T^4_{\rm max}})^{1/2}, \quad (4)$$

where $F^{\rm obs}_{\rm BB}$ is observed total flux of the mBB component, and σ is the Stefan's constant. The radius of the

photosphere can be estimated with

$$R_{\rm ph} = [\frac{\sigma_T L_0 D_{\rm L}^3}{8\pi m_{\rm p} c^3 (1+z)^6} (\frac{F_{\rm BB}^{\rm obs}}{\sigma T_{\rm max}^4})^{3/2}]^{1/4}, \quad (5)$$

where L_0 is a total luminosity of both the thermal and non-thermal emission.

The derived $\Gamma_{\rm ph}$ and $R_{\rm ph}$ values are reported in Table 2. It is found that the $\Gamma_{\rm ph}$ value in the Episode I is 175. During Episode II, initially, the $\Gamma_{\rm ph}$ is 1162 in the time slice of [180-187] seconds. Then, it rapidly goes up to 2274 at the time slice of [188-189] seconds, and goes down and keeps at about 800-1100 in the late slices. The $R_{\rm ph}$ value increases from 1.52×10^{10} cm to 2.66×10^{11} cm, then keeps in the range of $(2.66-3.76)\times10^{11}$ cm. The temporal evolution of $\Gamma_{\rm ph}$ and $R_{\rm ph}$ value are shown in bottom panel of Figure 4. The extremely large Lorentz factor may make this event extremely bright (e.g., Liang et al. 2010; Wu et al. 2011).

4.2. *Jet Properties Derived from the Afterglow Data*

As mentioned in §3.2, the late afterglow data is consistent with the prediction of the standard afterglow models. We derive the jet properties from the afterglow data in this section. The details of our model and fitting strategy please refer to Huang et al. (2016). With the observed spectral index and temporal decay slope of the normal decay segment (from 10^5 to 10^6 seconds), we suggest that both the optical and X-ray emission should be in the spectral regime between ν_m and ν_c, and take $p = 2\beta + 1 \sim 2.4$, where we take $\beta \sim 0.70$ derived from the time slice $[1.5-2.0]\times10^5$ seconds. The fractions of internal energy converted to the electrons and magnetic field are $\varepsilon_{\rm e,r}$ and $\varepsilon_{\rm B,r}$ in the reverse shock region, and $\varepsilon_{\rm e,f}$ and $\varepsilon_{\rm B,f}$ are in the forward shock region. We assume that the medium surrounding the jet is the interstelar medium (ISM) with a constant density (n). The temporal evolution of both minimum and cooling frequencies (ν_m and ν_c) in the reverse and forward shock regions are taken from Rossi et al. (2003), Fan & Piran (2006), Zhang et al. (2007) and Yi et al. (2013). We use an Markov Chain Monte Carlo (MCMC) technique to make the best fit to the observed lightcurves. The details of the technique and our procedure please refer to Huang et al. (2016). We derive $\epsilon_{\rm e,r} = 0.16\pm0.02$, $\epsilon_{\rm e,f} = 0.10\pm0.01$, $\epsilon_{\rm B,r} \sim 4\times10^{-5}$, $\epsilon_{\rm B,f} = (1.82\pm0.47)\times10^{-7}$, $n \sim 36$ cm^{-3}, the fireball kinetic energy $E_{\rm K,iso} = (1.72\pm0.12)\times10^{55}$ erg, the initial fireball Lorentz factor $\Gamma_0 = 116\pm4$, and jet opening angle $\theta_{\rm j} = 12^\circ\pm2^\circ$. Defining a magnetization parameter as $R_B \equiv \epsilon_{\rm B,r}/\epsilon_{\rm B,f}$, one has $R_B \sim 222$. It is lower than that of GRBs 990123, 090102, 130427A and 140512A, whose early optical emission is dominated by the reverse emission (Gao et al. 2015; Huang et al. 2016). Our results are shown in Figure 7. One can observe that the optical emission of the first three data point in the time interval [195, 205] seconds is dominated by a bright optical flare. The segment with a decaying slope of -3.57 ± 0.09 is dominated by the reverse shock emission. Late optical and X-ray afterglow since $t > 10^4$ seconds are contributed by the forward shock emission.

5. DISCUSSION

Three well separated emission episodes observed in GRB 160625B have distinct spectral properties. This may shed light on the evolution of the outflow and even the activity of the GRB central engine. In this section, we discuss possible physical origins of these distinct emission episodes and implications for the central engine of GRB 160625B.

5.1. *Episode I: Emission of the Cocoon Surrounding the Jet?*

Episode I is a short precursor with following long quiescent stage. Hu et al. (2014) made an analysis for a large sample of GRB lightcurves observed with *Swift* Burst Alert Telescope (BAT) in order to search for the possible precursor emission prior to the main outbursts. They found that about 10% long GRBs have a precursor emission component. Most of precursors show as continuous fluctuations with low flux level. Being due to the narrowness of the BAT band, they fitted the spectra of both the precursors and the main outbursts. They found that their photon indices do not show any statistical difference and suggested that the precursor would be the same emission component from the fireball (see also Lazzati, 2005; Burlon et al. 2008). The emission of Episode I of GRB 160625B is dramatically different from these precursors. Its spectrum is well fitted with a mBB model. In addition, it is very short and bright. Figure 9(a) compares Episode I of GRB 160625B with precursors of some *Swift* GRBs in the plane of the hardness ratio (HR) vs. the duration of the precursors $T_{\rm pre}$, where HR is the ratio of photon fluxes between the 50-100 keV and 15-150 keV bands. It is found that the emission of Episode I is significantly harder than that of the *Swift* GRBs. The peak fluxes of the precursors of these *Swift* GRBs are also tightly corrected with that of the main outbursts, but the emission in Episode I deviates this correlation, as shown in Figure 9(b). The peak flux of Episode I of GRB 160625B is much brighter than other *Swift* GRBs. After the end of Episode I, no signal was detected by GBM and LAT until the Episode II comes. Although tail emission of Episode I may be detectable with *Swift*/XRT as usually seen in some GRBs (e.g., Peng et al. 2014), the rapid cease of this Episode and a long quiescent stage may indicate the rapid close of this emission channel. Therefore, the physical origin of emission in Episode I may hold the key to reveal the evolution of the GRB jet.

Several models were proposed to interpret the precursor emission of GRBs (Lyutikov & Usov 2000; Ramirez-Ruiz et al. 2002; Wang & Mészáros 2007; Bernardini et al 2013). It is believed that long GRBs are a relativistic fireball from collapses of massive stars. Lyutikov & Usov (2000) suggested that a weak precursor may attribute to the photosphere emission of the GRB fireball when it becomes transparent. In this scenario, spectrum of the precursor should be thermal or quasi-thermal. Our spectral analysis indicates that the spectrum of Episode I indeed can be fitted with the mBB model. In this scenario, our results likely suggest that the GRB fireball experienced an acceleration stage from Episode I to Epsode II when the fireball was expanded. However, the short duration of Episode I and long quiescent stage after Episode I are difficult to be explained with this scenario since the photosphere emission could not be rapidly shut up when the

fireball is transparent.

Ramirez-Ruiz et al. (2002) suggested that a cocoon surrounding a relativistic jet may be formed when the jet breaks out of the progenitor envelope. They assumed that the cocoon has the same Lorentz factor as the GRB jet and discussed possible photospheric "cooling emission" from the cocoon. This emission component may produce gamma-ray and X-ray transients with a short duration since this channel should be rapidly closed due to the drop of pressure. Lazzati et al.(2010) investigated the cocoon evolution and suggested that the transients may be seen similar to a short GRB by an observer at 45°. More recently, Nakar & Piran (2017) explored the possible signatures of the cocoon emission. They showed that the cocoon signature depends strongly on the level of mixing between the shocked jet and shocked stellar material. In case of no mixing at all, bright gamma-ray emission with a duration of seconds from the cocoon can be detectable with current missions, such as *Swift* and *Fermi*. Non-detection of such an emission component in most GRBs implies that indicates that such kind of mixing must take place. The spectrum and duration of emission in Episode I of GRB 1600625B seem to be consistent with the case of no mixing at all. This makes this GRB very valuable for revealing the progenitor and jet of this GRB (Nakar & Piran 2017).

5.2. *Episode II: Main Burst from the Jet?*

Our time-resolved spectral analysis for the emission in Episode II shows that the spectra are well fitted with the mBB+CPL model. Lü et al. (2017) present a systematical spectral fit for 37 bright GRBs simultaneously observed with GBM and LAT by invoking the mBB+CPL or mBB+PL models. They show that the spectra of 32 GRBs can be fitted with the mBB+CPL model, and the spectra of other 5 GRBs are adequately fitted with the mBB+PL model. Therefore, the gamma-ray emission of Episode II should be resemble typical LAT GRBs.

A bright optical flare was simultaneously detected in the Episode II. Based on our theoretically modeling with the forward and reverse shock models for the optical and X-ray data as shown in Figure 5, one can find that this flare is shaped by both the prompt optical emission and reverse shock emission, similar to that observed in GRB 140512A (Huang et al. 2016). By subtracting the contribution of the reversed shock emission, the optical flux at the peak time is scaled down a little bit to that extrapolated from the fitting result of the gamma-ray emission[5]. With the derived isotropic kinetic energy from our modeling for the afterglow data and the observed gamma-ray energy of Episode II, we also calculate the GRB radiation efficiency with $\eta_\gamma = E_{\gamma,\rm iso}/(E_{\gamma,\rm iso} + E_{\rm K,iso})$ and obtain $\eta_\gamma = (14.9 \pm 0.9)\%$. We compare the radiation efficiency of GRB 160625B with other GRBs (Racusin et al. 2011). It is also similar to typical long GRBs, as shown in Figure 10.

5.3. *Episode III: Extended emission and high energy afterglow emission?*

From Figure 1, one can observe that the emission of this episode is clearly detected with GBM-NaI and LAT. The lightcurve observed with NaI features as the extended emission in most GRBs (Hu et al. 2014), but the LAT light curve of this episode steady increase right after the end of the Episode II. The spectrum of Episode III is shown in Figure 6, which also suggests that they should be different emission components. The spectrum observed with LAT should be distinct spectral component from the spectrum observed with GBM. It is well fit with a single power-law with an index of 1.98 ± 0.5. This component is similar to the extra power-law component observed in GRBs 090902B and 990510 (Ryde et al. 2010; Zhang et al. 2011). We suspect that this component is the high energy afterglows produced in the forward region and the steady increase of the LAT flux could be the onset of the high energy afterglows (e.g., Ghisellini et al. 2010).

6. CONCLUSIONS

GRB 160625B is an extremely bright GRB with measured redshift $z = 1.406$. The light curve of prompt emission is composed of three distinct episodes: a short precursor (Episode I), a very bright main emission episode (Episode II), and a weak emission episode, (Episode III). Those three episodes emission are separated by two quiet period of ~ 180 and ~ 300 seconds, respectively. The total isotropic-equivalent energy ($E_{\gamma,iso}$) and peak luminosity ($L_{\rm iso}$) are as high as $\sim 3 \times 10^{54}$ erg and $\sim 4 \times 10^{53}$ erg s^{-1}, respectively. The early optical emission is very bright with 8.04 magnitude during the main emission episode. By analyzing its data observed with the GBM and LAT on board the *Fermi* mission, we find the following interesting results:

- The emission of Episode I is significantly harder than that of the *Swift* GRBs. The spectrum of Episode I can be fitted with a mBB model, and the derived maximum temperature ($kT_{\rm max}$) is ~ 25 keV. Those features suggest that the Episode I is different from other *Swift* GRBs detected precursors. We propose that the emission of Episode I seems to be from the emission of cocoon surrounding the jet with the case of no mixing between shocked jet cocoon and shocked stellar cocoon.

- An extremely bright of Episode II has a higher isotropic-equivalent energy, and the time-resolved spectral analysis for the emission in Episode II shows that the spectra are well fitted with a model composing of an mBB component plus a cutoff power-law component. The radiation efficiency of this Episode is similar to other typical long GRBs. Those features suggest that the emission of Episode II is contributed by both photosphere emission and internal shock of relativistic jet.

- The spectrum of Episode III is adequately fitted with a CPL plus a single power-law models, and no mBB component is required. This may imply that the emission Episode III is contributed by both internal and external shocks of relativistic jet.

- The early and later afterglows are consistent with reverse and forward shock models, respectively.

[5] This situations may be caused by two possible reasons. One is regarding the uncertainty extrapolated from γ-ray to optical band. Another one may have different radiation mechanisms between γ-ray and optical emission

Derived the initial fireball Lorentz factor $\Gamma_0 = 116 \pm 4$, and jet opening angle $\theta_{\rm j} = 12^\circ \pm 2^\circ$.

We acknowledge the use of the public data from the *Fermi* and *Swift* data archive. This work is supported by the National Basic Research Program of China (973 Program, grant No. 2014CB845800), the National Natural Science Foundation of China (Grant No. 11603006, 11663002, 11533003, 11363002), the Guangxi Science Foundation (2016GXNSFCB380005, 2014GXNSFAA118011, 2014GXNSFBA118009, 2013GXNSFFA019001), the One-Hundred-Talents Program of Guangxi colleges, the high level innovation team and outstanding scholar program in Guangxi colleges, and Scientific Research Foundation of GuangXi University (Grant No XGZ150299).

REFERENCES

Band, D., Matteson, J., Ford, L., et al. 1993, ApJ, 413, 281
Beloborodov, A. M. 2010, MNRAS, 407, 1033
Bernardini, M. G., Campana, S., Ghisellini, G., et al. 2013, ApJ, 775, 67
Burlon, D., Ghirlanda, G., Ghisellini, G., et al. 2008, ApJ, 685, L19
Burns, E. 2016, GRB Coordinates Network, 19581, 1
Cash, W. 1979, ApJ, 228, 939
Dai, Z. G., & Lu, T. 1998, A&A, 333, L87
Dirirsa, F., Vianello, G., Racusin, J., & Axelsson, M. 2016, GRB Coordinates Network, 19586, 1
Fan, Y.-Z., Piran, T., & Xu, D. 2006, JCAP, 9, 013
Fan, Y., & Piran, T. 2006, MNRAS, 369, 197
Fruchter, A. S., Levan, A. J., Strolger, L., et al. 2006, Nature, 441, 463
Galama, T. J., Vreeswijk, P. M., van Paradijs, J., et al. 1998, Nature, 395, 670
Gao, H., Lei, W.-H., Zou, Y.-C., Wu, X.-F., & Zhang, B. 2013, NewAR, 57, 141
Gao, H., Wang, X.-G., Mészáros, P., & Zhang, B. 2015, ApJ, 810, 160
Geng, J.-J., Zhang, B., & Kuiper, R. 2016, ApJ, 833, 116
Ghisellini, G., Ghirlanda, G., Nava, L., & Celotti, A. 2010, MNRAS, 403, 926
Ghisellini, G., Ghirlanda, G., & Tavecchio, F. 2007, MNRAS, 375, L36
Giannios, D. 2008, A&A, 480, 305
Hu, Y.-D., Liang, E.-W., Xi, S.-Q., et al. 2014, ApJ, 789, 145
Huang, X.-L., Xin, L.-P., Yi, S.-X., et al. 2016, ApJ, 833, 100
Lü, H.-J., & Zhang, B. 2014, ApJ, 785, 74
Lü et al. 2017, in preparation.
Lazzati, D. 2005, MNRAS, 357, 722
Lazzati, D., & Begelman, M. C. 2010, ApJ, 725, 1137
Lazzati, D., & Begelman, M. C. 2005, ApJ, 629, 903
Lazzati, D., Morsony, B. J., & Begelman, M. C. 2010, ApJ, 717, 239
Lei, W.-H., Zhang, B., & Liang, E.-W. 2013, ApJ, 765, 125
Liang, E.-W., Yi, S.-X., Zhang, J., et al. 2010, ApJ, 725, 2209
Liang, E.-W., Zhang, B.-B., & Zhang, B. 2007, ApJ, 670, 565
Lundman, C., Pe'er, A., & Ryde, F. 2013, MNRAS, 428, 2430
Lyutikov, M., & Usov, V. V. 2000, ApJ, 543, L129
Mészáros, P., & Rees, M. J. 2000, ApJ, 530, 292
Mészáros, P., & Rees, M. J. 1997, ApJ, 476, 232
MacFadyen, A. I., & Woosley, S. E. 1999, ApJ, 524, 262
Meegan, C., Lichti, G., Bhat, P. N., et al. 2009, ApJ, 702, 791-804
Melandri, A., D'Avanzo, P., D'Elia, V., et al. 2016, GRB Coordinates Network, 19585, 1
Meszaros, P., Laguna, P., & Rees, M. J. 1993, ApJ, 415, 181
Mizuta, A., & Ioka, K. 2013, ApJ, 777, 162
Morsony, B. J., Lazzati, D., & Begelman, M. C. 2007, ApJ, 665, 569
Nakar, E., & Piran, T. 2017, ApJ, 834, 28
Narayan, R., Piran, T., & Kumar, P. 2001, ApJ, 557, 949
Paczyński, B. 1998, ApJ, 494, L45
Pe'er, A., Mészáros, P., & Rees, M. J. 2006, ApJ, 642, 995
Pe'er, A., & Ryde, F. 2011, ApJ, 732, 49
Pe'er, A., Ryde, F., Wijers, R. A. M. J., Mészáros, P., & Rees, M. J. 2007, ApJ, 664, L1
Peng, F.-K., Liang, E.-W., Wang, X.-Y., et al. 2014, ApJ, 795, 155
Piran, T., Shemi, A., & Narayan, R. 1993, MNRAS, 263, 861
Piro, L., Troja, E., Gendre, B., et al. 2014, ApJ, 790, L15
Popham, R., Woosley, S. E., & Fryer, C. 1999, ApJ, 518, 356
Racusin, J. L., Oates, S. R., Schady, P., et al. 2011, ApJ, 738, 138
Ramirez-Ruiz, E., Celotti, A., & Rees, M. J. 2002, MNRAS, 337, 1349
Rees, M. J., & Mészáros, P. 2005, ApJ, 628, 847
Rees, M. J., & Meszaros, P. 1994, ApJ, 430, L93
Rhoads, J. E. 1997, ApJ, 487, L1
Rossi, E., & Rees, M. J. 2003, MNRAS, 339, 881
Ryde, F., Axelsson, M., Zhang, B. B., et al. 2010, ApJ, 709, L172
Sari, R., Piran, T., & Narayan, R. 1998, ApJ, 497, L17
Stanek, K. Z., Matheson, T., Garnavich, P. M., et al. 2003, ApJ, 591, L17
Svinkin, D., Golenetskii, S., Aptekar, R., et al. 2016, GRB Coordinates Network, 19604, 1
Thompson, C. 1994, MNRAS, 270, 480
Troja, E., Rosswog, S., & Gehrels, N. 2010, ApJ, 723, 1711
Usov, V. V. 1992, Nature, 357, 472
Wang, X.-Y., & Mészáros, P. 2007, ApJ, 670, 1247
Wang, Y.-Z., Wang, H., Zhang, S., et al. 2016, arXiv:1611.04879
Woosley, S. E. 1993, ApJ, 405, 273
Woosley, S. E., & Bloom, J. S. 2006, ARA&A, 44, 507
Wu, Q., Zou, Y.-C., Cao, X., Wang, D.-X., & Chen, L. 2011, ApJ, 740, L21
Xu, D., Malesani, D., Fynbo, J. P. U., et al. 2016, GRB Coordinates Network, 19600, 1
Yi, S.-X., Wu, X.-F., & Dai, Z.-G. 2013, ApJ, 776, 120
Zhang, B.-B., Zhang, B., Castro-Tirado, A. J., et al. 2016, arXiv:1612.03089
Zhang, B.-B., Zhang, B., Liang, E.-W., et al. 2011, ApJ, 730, 141
Zhang, B., & Kobayashi, S. 2005, ApJ, 628, 315
Zhang, B., Liang, E., Page, K. L., et al. 2007, ApJ, 655, 989
Zhang, B., & Yan, H. 2011, ApJ, 726, 90
Zhang, W., Woosley, S. E., & MacFadyen, A. I. 2003, ApJ, 586, 356

TABLE 1
Time-resolved Spectral fitting with mBB+CPL models for Episode II of GRB 160625B

Time interval (s)	mBB			CPL			PGSTAT/dof
	Normalization	$T_{\rm min}$ (keV)	$T_{\rm max}$ (keV)	q	Γ_c	$E_{\rm c}$ (MeV)	
[180 ∼ 187]	$0.27^{+0.05}_{-0.05}$	$15^{+1.20}_{-1.20}$	643^{+68}_{-68}	$0.90^{+0.04}_{-0.04}$	$1.27^{+0.02}_{-0.02}$	$12.11^{+0.83}_{-0.83}$	310/271
[187 ∼ 188]	$5.34^{+0.24}_{-0.25}$	$30^{+0.26}_{-0.68}$	871^{+49}_{-27}	$0.81^{+0.03}_{-0.02}$	$1.31^{+0.02}_{-0.01}$	$17.19^{+3.40}_{-2.86}$	276/273
[188 ∼ 189]	$70.09^{+7.27}_{-3.07}$	$32^{+0.38}_{-0.36}$	1096^{+22}_{-23}	$0.64^{+0.02}_{-0.01}$	$1.34^{+0.02}_{-0.01}$	$16.59^{+1.03}_{-0.71}$	369/274
[189 ∼ 190]	$106.95^{+8.61}_{-7.65}$	$25^{+0.48}_{-0.48}$	940^{+40}_{-20}	$0.60^{+0.02}_{-0.02}$	$1.50^{+0.02}_{-0.03}$	$23.09^{+3.78}_{-3.63}$	362/270
[190 ∼ 191]	$64.57^{+8.17}_{-10.83}$	$17^{+0.29}_{-1.36}$	659^{+7}_{-66}	$0.59^{+0.02}_{-0.02}$	$1.60^{+0.04}_{-0.02}$	$26.97^{+6.40}_{-7.36}$	318/271
[191 ∼ 192]	$23.64^{+0.65}_{-1.12}$	$7^{+0.69}_{-1.44}$	260^{+56}_{-25}	$0.68^{+0.01}_{-0.01}$	$1.52^{+0.02}_{-0.02}$	$8.75^{+0.96}_{-0.95}$	299/254
[192 ∼ 193]	$19.69^{+0.60}_{-0.43}$	$5^{+1.25}_{-0.73}$	254^{+41}_{-18}	$0.72^{+0.01}_{-0.01}$	$1.47^{+0.02}_{-0.01}$	$7.64^{+0.69}_{-0.84}$	305/278
[193 ∼ 194]	$13.10^{+0.34}_{-0.42}$	$13^{+2.09}_{-2.53}$	289^{+18}_{-26}	$0.92^{+0.02}_{-0.04}$	$1.50^{+0.01}_{-0.01}$	$10.35^{+0.96}_{-0.85}$	296/276
[194 ∼ 195]	$20.29^{+3.03}_{-1.68}$	$12^{+1.62}_{-1.37}$	350^{+34}_{-27}	$0.86^{+0.06}_{-0.03}$	$1.53^{+0.02}_{-0.08}$	$12.07^{+1.01}_{-0.91}$	315/275
[195 ∼ 196]	$10.60^{+1.83}_{-0.69}$	$10^{+1.57}_{-2.18}$	287^{+25}_{-36}	$1.02^{+0.02}_{-0.08}$	$1.38^{+0.02}_{-0.03}$	$7.60^{+0.61}_{-0.49}$	307/275
[196 ∼ 197]	$9.42^{+0.17}_{-0.18}$	$9^{+0.04}_{-0.04}$	252^{+4}_{-7}	$1.01^{+0.01}_{-0.01}$	$1.40^{+0.02}_{-0.02}$	$7.79^{+0.86}_{-0.65}$	362/275
[197 ∼ 198]	$11.41^{+2.60}_{-1.96}$	$7^{+1.49}_{-1.43}$	338^{+27}_{-22}	$0.94^{+0.05}_{-0.05}$	$1.69^{+0.17}_{-0.08}$	$53.48^{+78.94}_{-26.89}$	287/272
[198 ∼ 199]	$9.24^{+3.07}_{-1.18}$	$10^{+2.14}_{-1.10}$	292^{+52}_{-6}	$0.98^{+0.01}_{-0.03}$	$1.54^{+0.05}_{-0.04}$	$16.11^{+5.05}_{-4.08}$	283/275
[199 ∼ 200]	$7.72^{+2.69}_{-1.47}$	$8^{+2.28}_{-1.63}$	338^{+34}_{-20}	$1.05^{+0.06}_{-0.06}$	$1.51^{+0.09}_{-0.06}$	$10.44^{+0.67}_{-1.36}$	250/275

TABLE 2
The Derived Properties of the Episodes II

Time Interval (s)	$F_{\rm BB}^{\rm obs}$ [a]	$F_{\rm non-BB}^{\rm obs}$ [a]	$\Gamma_{\rm ph}$ [b]	$R_{\rm ph}$ [c]
[180 ∼ 187]	0.11	0.22	1162	0.15
[187 ∼ 188]	1.54	2.41	1798	0.50
[188 ∼ 189]	8.98	6.42	2274	0.96
[189 ∼ 190]	10.11	4.19	2035	1.24
[190 ∼ 191]	4.64	1.81	1540	1.29
[191 ∼ 192]	1.45	0.99	878	2.66
[192 ∼ 193]	1.43	1.13	879	2.78
[193 ∼ 194]	2.57	1.19	959	3.13
[194 ∼ 195]	3.57	1.55	1095	2.87
[195 ∼ 196]	3.37	1.62	992	3.76
[196 ∼ 197]	2.49	1.01	883	3.74
[197 ∼ 198]	2.93	0.20	975	2.48
[198 ∼ 199]	2.47	1.05	953	2.98
[199 ∼ 200]	3.39	0.76	1028	2.81

[a] The observed total flux of mBB component and non-thermal component, respectively. The flux is in units of 10^{-5} erg cm^{-2} s^{-1}.
[b] The Lorentz factor of GRB photosphere.
[c] The radius of the photosphere in unit of 10^{11} cm.

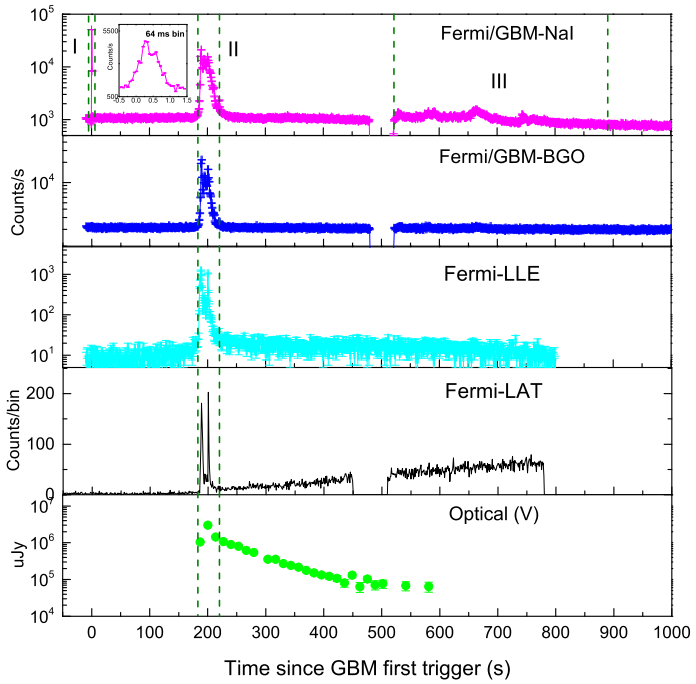

FIG. 1.— Prompt emission Light curves in different energy bands with one second time-bin. The inset in the top panel shows the temporal structure in 64 milliseconds bin. The vertical lines mark the episodes according to the light curve observed with GBM-NaI.

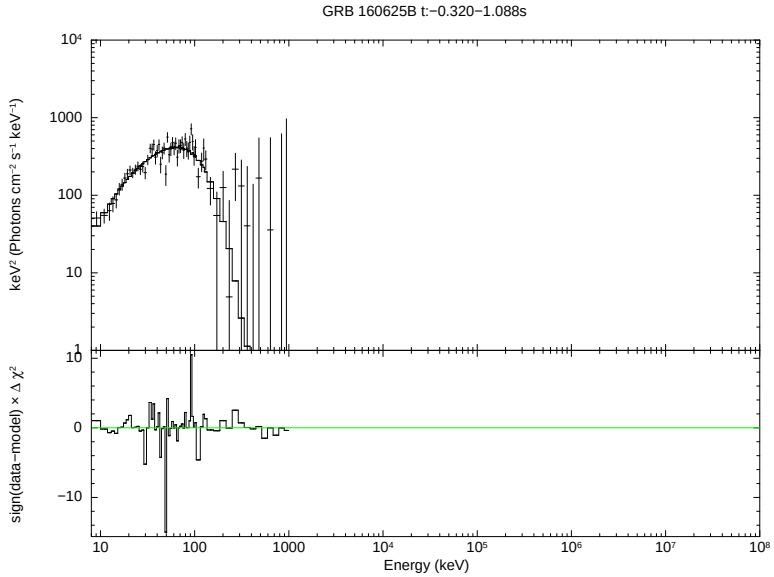

FIG. 2.— Time-integrated νf_ν spectrum of the emission Episode I together with our fit by using the mBB model (solid line).

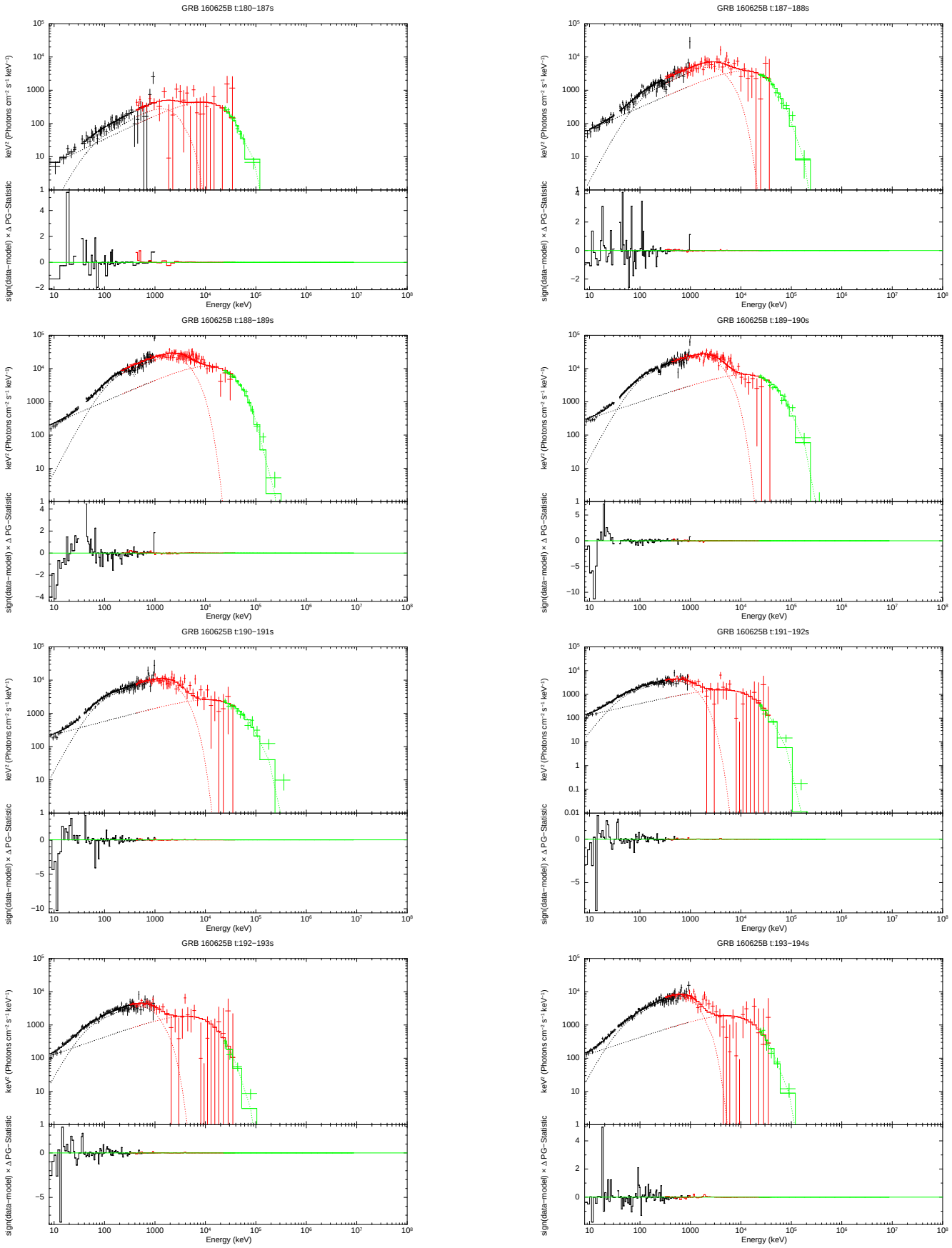

FIG. 3.— Observed time-resolved νF_ν spectra of the emission Episode II (the main emission episode) together with our fits with the mBB+CPL model (dot lines). Black points, red points, and green points are data observed with NaI, BGO and LAT, respectively.

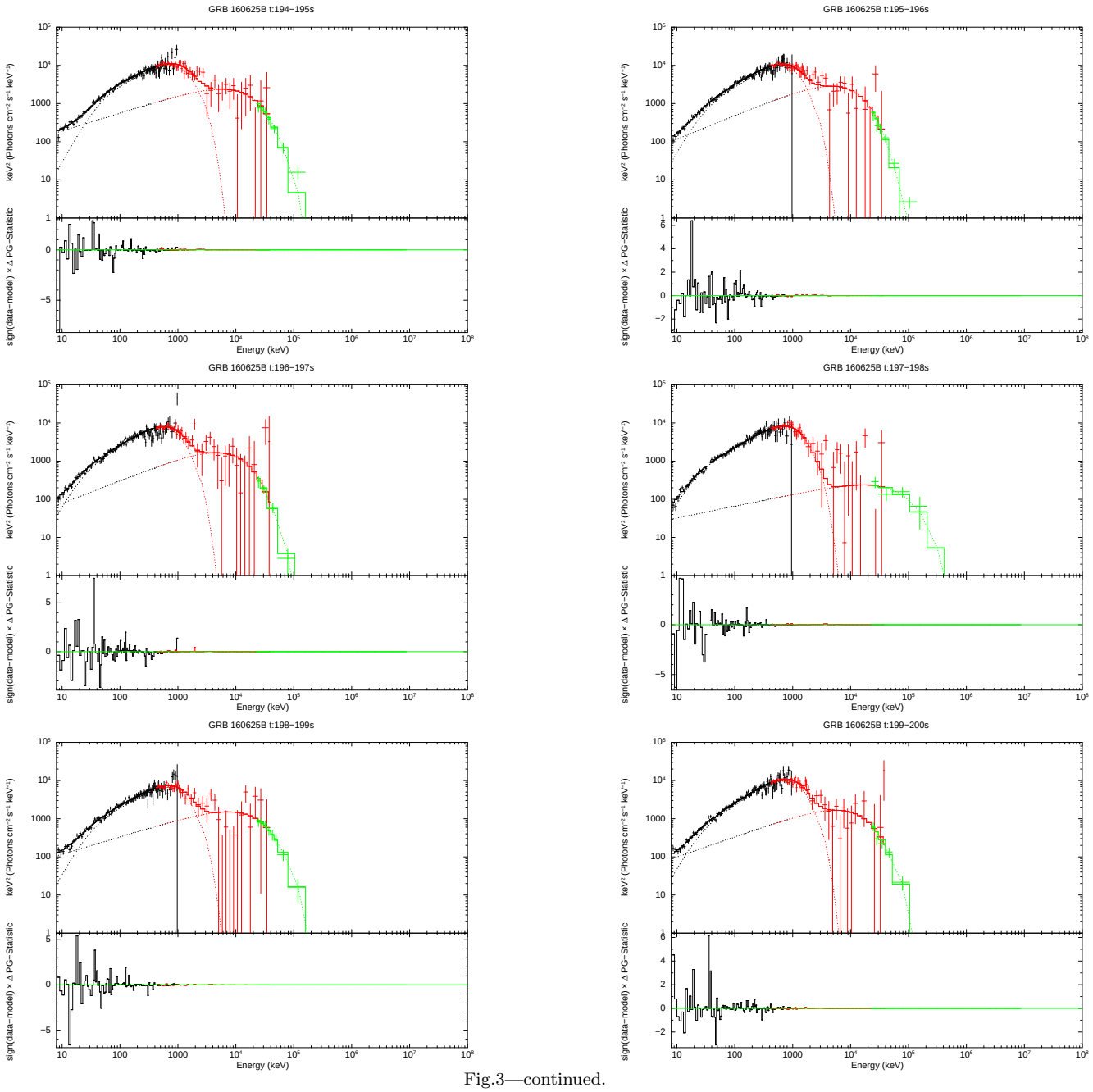

Fig.3—continued.

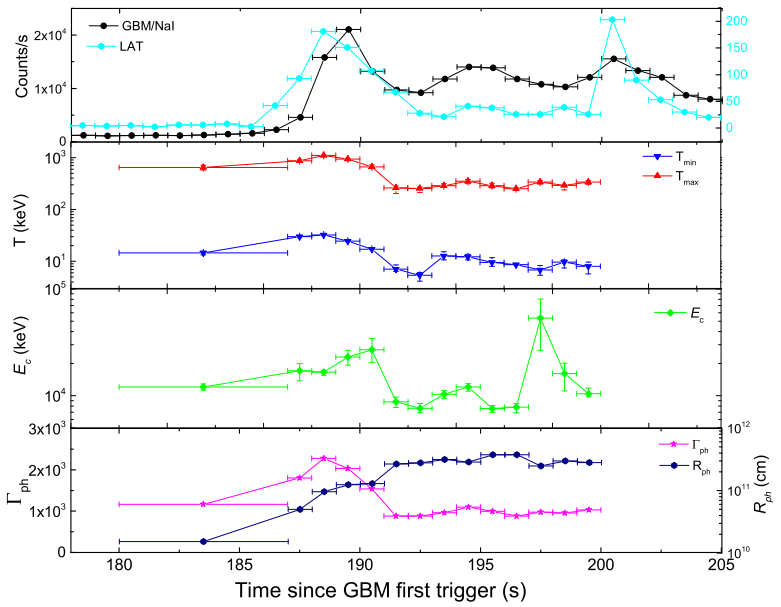

FIG. 4.— Temporal evolution of $T_{\rm min}$, $T_{\rm max}$, $E_{\rm c}$ and $\Gamma_{\rm ph}$ during Episode II. The top panel is the lightcurves of GBM/NaI and LAT.

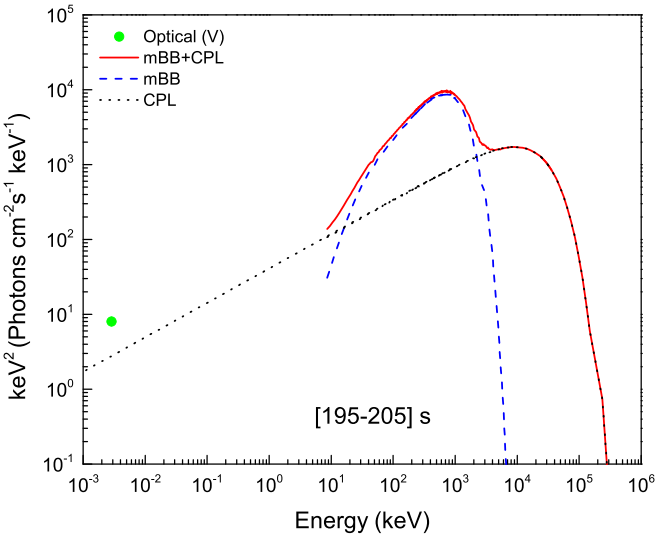

FIG. 5.— Model curves derived from our fit for the spectrum observed in the time slice [195-205] in comparison with the peak optical flux (the blue dot) in the same time interval, where the optical data is corrected by the extinction of the Milk Way Galaxy and removing the contribution of the reverse shock at this time, but is not corrected for the extinction by the GRB host galaxy.

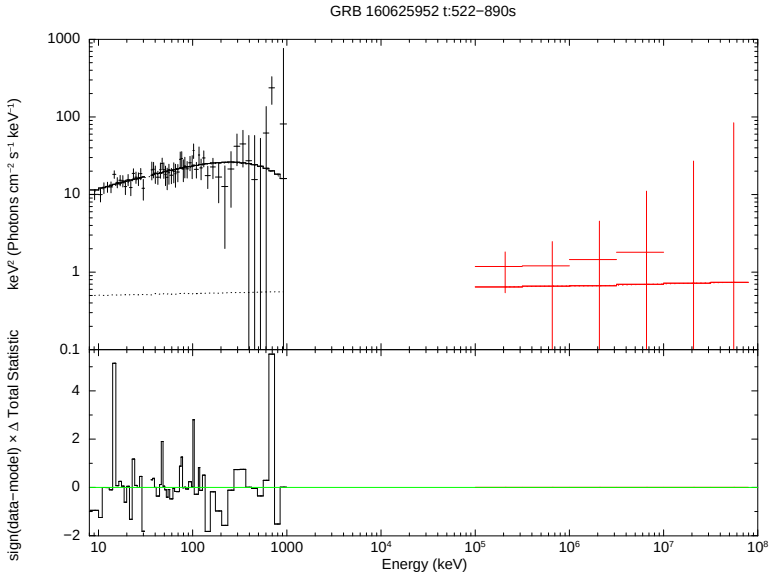

FIG. 6.— Time-integrated spectrum of the emission Episode III together with our fit by using the CPL+PL model (solid line).

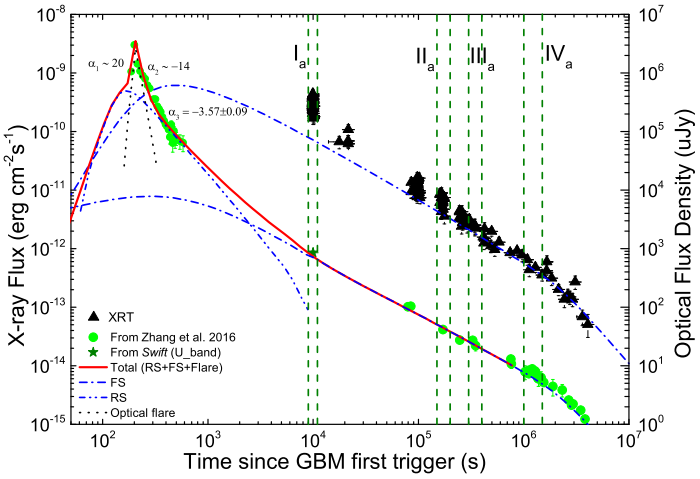

FIG. 7.— Lightcurves of the prompt optical, early and later optical afterglow, and X-ray afterglow of GRB 160625B. The red line is our model fit with the external shock model, in which the reverse shock and forward shock emission components are represented with the dash-dotted and dash-dot-dotted lines, respectively. The extremely sharp optical pulse of the first three optical data points are suggested to be dominated by the prompt optical flare (black dotted lines). The vertical dashed lines make the selected time slices of our spectral analysis.

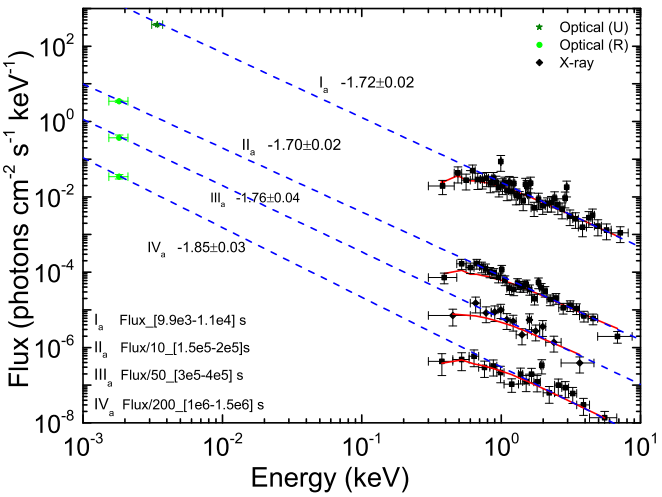

FIG. 8.— Spectral energy distributions of the Optical-X-ray emission in four selected time intervals. Dashed lines are the spectra fitting with absorbed power-law functions that are extrapolated to the optical bands.

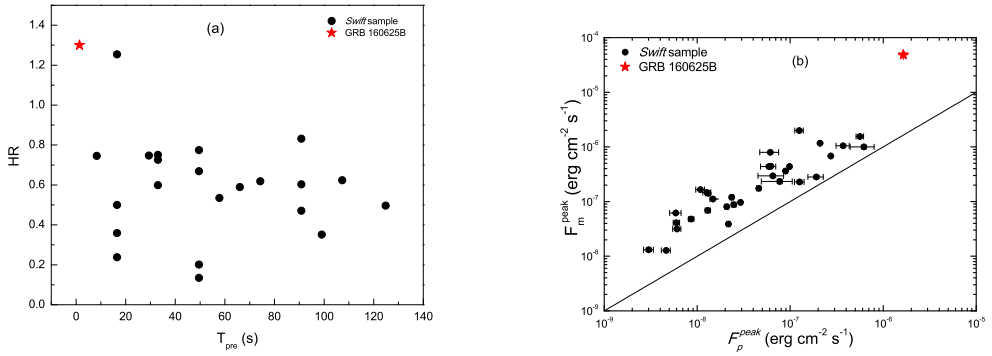

FIG. 9.— (a): Hardness ratio (HR) as function of precursors duration ($T_{\rm pre}$). (b) Peak flux of main bursts ($F_{\rm m}^{\rm peak}$) as function of Peak flux of precursors ($F_{\rm p}^{\rm peak}$). Black solid circle and red solid star are *Swift* sample detected precursors and GRB 160625B. The solid line is corresponding to equal peak flux between precursors and main bursts.

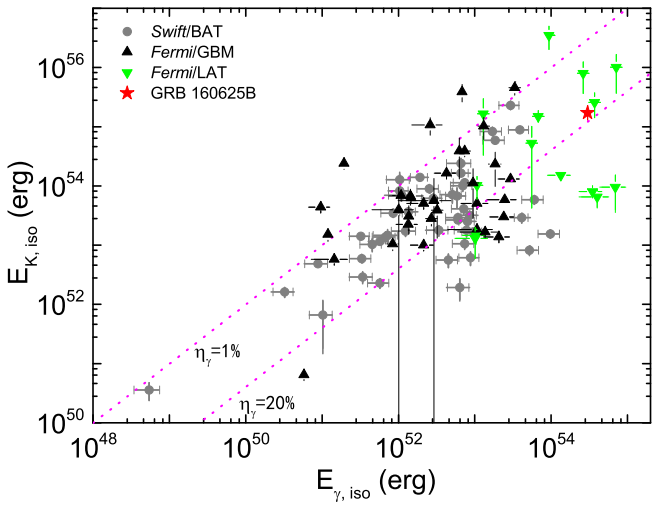

FIG. 10.— $E_{\gamma,\rm iso}$ as function of $E_{\rm K,iso}$ for *Swift*/BAT (gray dots), *Fermi*/GBM (black triangles), *Fermi*/LAT (green triangles) and GRB 160625B (red star) with redshift measurements (Racusin et al. 2011). The dotted lines mark the constant γ-ray efficiency (η_γ) lines.